Predictive Ice Accretion Control on ML driven Superhydrophobic Surface Design for Aerospace Applications

*Kshitija Vaidya[a], Balasubramanian Kandasubramanian[a]**
[a]Department of Metallurgical and Materials Engineering,
Defence Institute of Advanced Technology (DU), Girinagar, Pune – 411025
**Corresponding author email id.: meetkbs@gmail.com*

doi: https://doi.org/10.37285/bsp.SACAD2025.63

Abstract- Conventional electrothermal and chemical de-icing systems are inherently reactive, power-intensive, and susceptible to thermal degradation, underscoring the need for low interfacial toughness materials that enable passive, energy-efficient ice mitigation. In this regard, this investigative research identifies ultra-high-molecular-weight polyethylene (UHMWPE) as a compelling alternative owing to its low density, exceptional cryogenic toughness, low surface energy, and chemical inertness, ensuring weight efficiency and stable operation under extreme aerospace environments. Laser-induced hierarchical micro–nano structuring transformed UHMWPE into a bioinspired super hydrophobic interface, exhibiting a static contact angle of 149.7°, a roll-off angle of 3.1°, and a 61% reduction in surface free energy relative to the pristine polymer. The textured surface sustained low hysteresis (<5°) and preserved Cassie–Baxter wetting after 60 wetting cycles and freeze–thaw exposure, confirming superior mechanical and thermodynamic resilience. Random Forest and Temporal Convolutional Network (TCN) models trained on contact-angle data predicted degradation kinetics, maintenance intervals, and ice-initiation probabilities with high accuracy (R^2 = 0.94–0.96). The integration of surface-engineered UHMWPE with machine learning–driven predictive maintenance establishes a durable, adaptive anti-icing skin architecture for next-generation aerospace platforms.

Keywords- Ultra-high molecular weight polyethylene, machine learning, aerospace, Anti-icing, bio-inspired, superhydrophobic

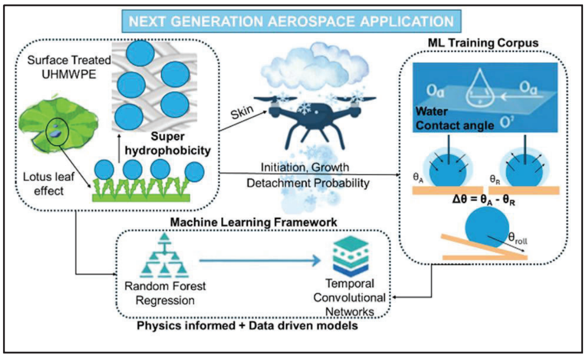

I. INTRODUCTION

Ice accretion on aerodynamic surfaces originates from the impact and subsequent freezing of supercooled water droplets, producing heterogeneous ice layers that disrupt local flow fields, alter boundary layer transition, and significantly degrade lift, drag, and control stability. The resulting changes in surface topology and pressure distribution can cause premature stall, rotor imbalance, and sensor malfunction, thereby constraining the operational performance of aerial vehicles.[1] Conventional mitigation methods, including electrothermal heating, hot air bleed systems, pneumatic boots, and glycol-based fluid application, remain predominantly reactive and thermally inefficient. Electrothermal systems demand high electrical power, create spatially nonuniform temperature fields, and introduce cyclic thermal stress that accelerates material fatigue. Pneumatic and mechanical systems add weight and mechanical complexity while providing intermittent protection. Hot air diversion reduces engine efficiency, whereas chemical fluids present environmental and maintenance challenges.[2], [3], [4] These limitations render traditional approaches unsuitable for small or energy limited unmanned aerial vehicles and next generation aerospace systems. As an alternative, surface coatings have been explored to passively resist ice adhesion through chemical modification or nanostructuring.

Passive de-icing coatings mitigate interfacial freezing by attenuating the adhesive interactions between ice and the substrate, even when the macroscopic rate of ice accretion remains largely unaltered[5]. Among the principal classes of materials employed for this purpose, polydimethylsiloxane (PDMS) and polytetrafluoroethylene (PTFE) are distinguished by their intrinsically low surface free energies and weak interfacial bonding with crystalline ice[6]. These polymers have demonstrated exceptionally low shear and tensile ice adhesion strengths across diverse coating configurations, including conformal thin films, self-assembled monolayers, and lubricant-infused architectures. Zhu et al.[7] fabricated silicone-oil-infused icephobic surfaces that exhibited markedly reduced shear adhesion of cylindrical ice at −10 °C, while Liu et al.[8] developed fluorinated PDMS coatings capable of delaying ice nucleation and significantly lowering interfacial bonding strength. In addition, certain amphiphilic polymers with higher surface energy can achieve comparable ice release by establishing a nanometric interfacial water layer. Because the cohesive strength of a liquid–solid interface is substantially weaker than that of a solid–solid contact, this quasi-liquid interphase serves as a lubricating boundary that facilitates interfacial slippage and debonding. Zeng et al.[9] developed a porous PDMS-based low interfacial toughness coating in which increasing porosity simultaneously enhanced hydrophobicity and reduced interfacial toughness, leading to superior ice-release performance. Dhyani et al.[10] engineered optically transparent low interfacial toughness coatings composed of PDMS and polyvinyl chloride (PVC) for photovoltaic applications, demonstrating a concurrent reduction in both interfacial toughness and ice adhesion strength. Similarly, Yu et al.[11] fabricated durable PTFE particle-based low interfacial toughness coatings that sustained low interfacial toughness even after multiple icing and de-icing cycles, highlighting the mechanical resilience and long-term stability of the microstructured surface. Dijvejin et al.[12] reported hybrid advances through the design of an integrated de-icing system that combined low interfacial toughness coatings, localized resistive microheaters, and an embedded microwave resonator sensor to enable precise, energy-minimal ice removal. This architecture, composed of ultra-high-molecular-weight polyethylene (UHMWPE) matrices, exploited controlled interfacial fracture mechanics to achieve ice detachment without complete melting, thereby reducing thermal energy requirements by approximately an order of magnitude relative to conventional electrothermal systems.

Despite their demonstrated efficacy, both passive and low interfacial toughness coatings exhibit intrinsic limitations arising from mechanical degradation, environmental aging, and thermomechanical fatigue under cyclic icing conditions. Progressive loss of surface texture, contamination-induced wettability transition, and diminished interfacial fracture performance compromise long-term reliability.[13] Hybrid configurations integrating coatings with resistive or microwave-assisted elements, while energy efficient, introduce architectural complexity, localized thermal gradients, and integration constraints on lightweight aerospace substrates.[14], [15] In contrast, multifunctional adaptive skins represent an advanced materials–systems paradigm, wherein hierarchical super hydrophobicity, dielectric tunability, and self-healing elasticity are embedded within a continuous, conformal layer. Such skins enable real-time ice-state sensing, predictive actuation, and autonomous mitigation, offering a scalable, resilient, and structurally compliant route toward intelligent anti-icing architectures for next-generation aerospace platforms. Xu et al.[16] reported the development of a multifunctional, self-healing skin for UAVs capable of both anti-icing and real-time ice monitoring. The five-layer system integrates supramolecular PDMS-based elastomers, self-healing electrodes, and a fluoropolymer encapsulation that lowers the ice nucleation temperature to −28.4 °C and reduces ice adhesion strength to 33 kPa. The skin functions as a capacitive sensor, enabling continuous detection of frost and ice accumulation during flight. When attached to UAVs, it provides stable adhesion, low weight, and precise response under cold, humid, and windy conditions. Yang et al.[17] reported the design of ultralow-temperature-tolerant electronic skins for robotic applications in polar environments. The e-skin was constructed from PDMS-based supramolecular elastomers incorporating quadruple hydrogen-bonding (UPy) motifs, enabling extreme stretchability (~3257 %), high toughness, and self-healing capability at −78 °C. Side-chain UPy architectures provided lower binding-energy variation and enhanced molecular mobility, yielding superior mechanical and self-repairing performance. Although these supramolecular e-skins demonstrated remarkable multifunctionality, their complex chemistries and fabrication protocols limit scalability and cost efficiency.[18] Consequently, there arises a compelling impetus to develop simplified, polymer-based adaptive skins that retain functional versatility while ensuring manufacturability and affordability. Emulating the lotus-leaf archetype, engineered superhydrophobic architectures manifest hierarchical micro–nano textural order that entraps interfacial air and minimizes the thermodynamic wetted fraction. This morphological sophistication drastically attenuates surface free energy, impedes heterogeneous ice nucleation, and promotes spontaneous droplet mobility, thereby conferring an intrinsically energy-minimal and self-sustaining de-icing capability under cryogenic aerospace environments.[19]

This investigation articulates a seminal and economically pragmatic advancement in the field of intelligent anti-icing materials through the strategic employment of ultra-high-molecular-weight polyethylene (UHMWPE), a polymer distinguished by its extraordinary molecular weight (>3 × 10^6 g·mol^{-1}) yet low density, low glass transition temperature ($T_g \approx -150$ °C), melting point around 135–138 °C, and exceptional chemical and oxidative stability. These attributes confer outstanding cryogenic toughness, low moisture permeability, and dimensional stability under extreme thermomechanical and environmental stress, rendering UHMWPE particularly suitable for aerospace operations in sub-zero atmospheres. Through laser-induced hierarchical surface texturing, the polymer surface is transformed into a bioinspired superhydrophobic architecture, wherein micro- and nanoscale asperities emulate the lotus-leaf topology, minimizing surface free energy, suppressing heterogeneous ice nucleation, and promoting spontaneous droplet roll-off. The engineered surfaces were exclusively characterized through water contact angle (WCA) goniometry, encompassing static, advancing, receding, and roll-off angles to determine wetting hysteresis and apparent work of adhesion which serve as quantitative indicators of interfacial integrity and surface degradation. These descriptors were assimilated into a machine-learning (ML)-driven predictive maintenance framework, enabling data-centric evaluation of hydrophobic endurance and service life. The confluence of thermally stable polymer architecture, laser-enabled surface functionalization, and AI-assisted maintenance analytics defines a scalable, self-diagnostic, and energy-efficient paradigm for long-duration anti-icing and surface-lifecycle management in aerospace environments.

II. WETTING THERMODYNAMICS

Wetting theory delineates the thermodynamic and geometric principles that govern liquid–solid interfacial energetics, constituting the foundational framework for interpreting ice nucleation, accretion, and interfacial adhesion phenomena across engineered surfaces. At interfacial equilibrium, the vectorial balance of surface tensions is defined by Young's relation, which encapsulates the intrinsic equilibrium among the solid–vapor, solid–liquid, and liquid–vapor interfacial energies [20],

$\gamma_{sv} - \gamma_{sl} = \gamma_{lv} cos\theta_Y$ … (eq. 1)

where γ_{ij} denote the solid–vapor, solid–liquid, and liquid–vapor interfacial tensions, and θ_Y represents the intrinsic (Young) contact angle. The work of adhesion, expressing the reversible energy required to separate a unit area of liquid from the solid, follows Dupre's relation:

$W_{sl} = \gamma_l (1 + cos\theta)$ … (eq. 2)

Surface morphology profoundly modifies wetting by altering the effective contact area and liquid–solid fraction. In the Wenzel regime, where liquid penetrates asperities, the apparent contact angle becomes

$cos\theta^* = r cos\theta_Y$ …(eq. 3)

with r as the roughness ratio. Conversely, in the Cassie–Baxter regime, where trapped air pockets coexist beneath the liquid,

$cos\theta^* = \emptyset_s(cos\theta_Y + 1) - 1$ …(eq. 4)

where ϕ_s is the solid–liquid contact fraction. High apparent angles ($\theta^* > 150°$) and low contact-angle hysteresis $\Delta\theta = \theta_A - \theta_R$ indicate superhydrophobicity and low droplet retention. The lateral retention force resisting droplet mobility is approximated by[21]

$F_{ret} = \pi D \gamma_{lv}(cos\theta_R - cos\theta_A)$ …(eq. 5)

where D denotes the droplet base diameter.

In the context of ice accretion, wetting thermodynamics dictate both heterogeneous ice nucleation kinetics and subsequent ice adhesion. The free energy barrier for heterogeneous nucleation relative to homogeneous freezing, ΔG^*_{het}, is reduced by a geometric factor $f(\theta_i)$ dependent on the ice–substrate contact angle θ_i:

$\Delta G^*_{het} = f(\theta_i)\Delta G^*_{hom}$ …(eq. 6)

$f(\theta_i) = \frac{(2+cos\theta_i)(1-cos\theta_i)^2}{4}$ …(eq. 7)

An increase in θ_i (corresponding to low wettability toward supercooled water) amplifies the energy barrier, thereby retarding nucleation and delaying frost initiation. During growth, the adhesive shear stress of ice, τ_{ice}, scales with interfacial work of adhesion and mechanical interlocking; minimizing W_{sl} and maintaining Cassie-type topography effectively lower τ_{ice}. Consequently, surfaces exhibiting high θ^*, low $\Delta\theta$, and stable Cassie states under condensation demonstrate reduced droplet residence time, inhibited heterogeneous nucleation density, and suppressed ice accretion rates, establishing wetting control as a first-order design parameter in anti-icing surface engineering[22].

III. MATERIALS & METHODS

A. Materials

For the present investigation, UHMWPE fibers of Dyneema SK78 grade were procured from DEBEL, Bengaluru, India.

B. Texturing of UHMWPE

Super hydrophobicity was imparted onto the UHMWPE surface through laser-induced surface texturing using an Nd:YAG laser system (EKSPLA NT 373). The laser operated at a wavelength of 1064 nm with a pulse energy of 246 mJ, a repetition rate of 10 Hz, and an exposure duration of 20 minutes[23].

C. Characterization

The wettability and interfacial properties of pristine and laser-textured UHMWPE surfaces were characterized using a contact angle goniometer (Krüss GmbH, DSA25, Germany) following the ASTM D7334–08 standard procedure for sessile drop analysis. Measurements were performed using deionized water droplets (5 ± 0.2 μL) dispensed at a controlled rate to minimize kinetic effects. The static contact angle (θ_s) and advancing (θ_A), and receding (θ_R) angles were determined by the dynamic sessile drop method under ambient conditions. The roll-off angle (θ_{roll}) was obtained by tilting the sample stage at a constant rate of 1° s^{-1} until droplet detachment occurred, in accordance with ASTM D724–99 guidelines. The apparent work of adhesion (WA) was computed using the Young–Dupré equation 2, [24]

D. Development of Machine Learning Model

To enable predictive assessment and maintenance forecasting of the superhydrophobic performance and surface longevity of laser-textured UHMWPE, machine learning (ML) algorithms were developed using datasets derived exclusively from WCA measurements.

1. Random Forest: A Random Forest (RF) regression model was developed using consolidated WCA datasets encompassing all measured wettability descriptors. Data preprocessing included normalization, outlier removal, and feature scaling to ensure statistical uniformity. The dataset was partitioned into 80% training and 20% validation subsets, and tenfold cross-validation was applied to optimize hyperparameters such as tree depth, number of estimators, and minimum leaf size. Feature permutation and Gini importance analysis identified the most influential parameters governing superhydrophobic retention, with contact-angle hysteresis and roll-off angle emerging as the dominant predictors. The optimized RF model exhibited stable convergence and accurate forecasting of hydrophobic degradation rate and maintenance intervals under varying environmental conditions.[25], [26]

2. Temporal Convolutional Networks: To capture the temporal evolution of surface wettability and degradation during repeated environmental exposure, a Temporal Convolutional Network (TCN) was constructed using sequential WCA data recorded over successive testing intervals. Prior to training, missing data points were interpolated using spline smoothing, and all temporal sequences were normalized and synchronized. The TCN architecture incorporated causal one-dimensional convolutional layers with residual connections, dilation factors of 1–8, and a kernel size of 3, enabling the network to learn both short- and long-term degradation trends. The model was trained using the Adam optimizer (learning rate = 0.001) and mean-squared error loss, with dropout and early stopping employed to prevent overfitting. The trained TCN successfully predicted future degradation trajectories, loss of super hydrophobicity, and maintenance requirements with high temporal accuracy. Integration with the RF model established a hybrid predictive maintenance framework, enabling real-time health monitoring and performance forecasting of the laser-engineered UHMWPE superhydrophobic skins.[27], [28]

IV. RESULTS & DISCUSSION

A. Water Contact Angle

The pristine UHMWPE surface exhibited a static contact angle of 130.5°, a roll-off angle of 7.4° as consolidated in table 1, and an apparent work of adhesion of 25.5 mN·m^{-1} calculated per equation 1, signifying a moderately hydrophobic character governed by strong solid–liquid interfacial interactions typical of the Wenzel regime. In contrast, the laser-textured UHMWPE displayed a markedly higher static contact angle of 149.7°, a significantly reduced roll-off angle of 3.1°, and a lower work of adhesion of 9.9 mN·m^{-1}, indicating a transition to a superhydrophobic Cassie–Baxter state.[29]

The hysteresis profile illustrated in Figure 1 exhibited a marked attenuation in contact-angle hysteresis, signifying minimal contact-line pinning and enhanced droplet mobility. Hysteresis values were systematically recorded for 60 consecutive sessile water droplets (5 ± 0.2 µL each) to assess the persistence of superhydrophobic functionality under repetitive wetting stress. Remarkably, the laser-textured UHMWPE surface sustained a stable Cassie–

TABLE 1: COMPARATIVE ANALYSIS OF WATER CONTACT ANGLE

<table>
<tr><th></th><th>Static Contact Angle (θ_s)</th><th>Roll Off Angle (θ_{roll})</th></tr>
<tr><td>1. Pristine</td><td>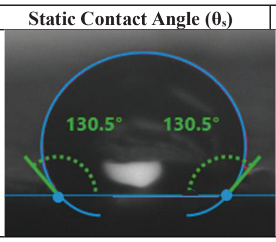
</td><td>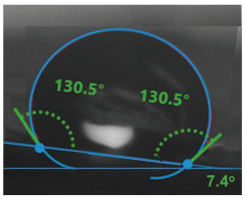
</td></tr>
<tr><td>2. Laser Textured</td><td>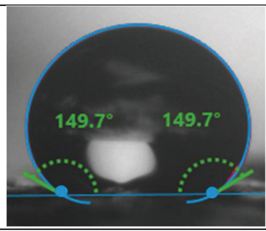
</td><td>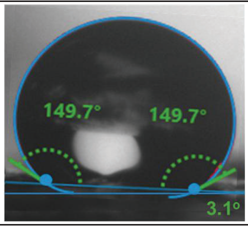
</td></tr>
</table>

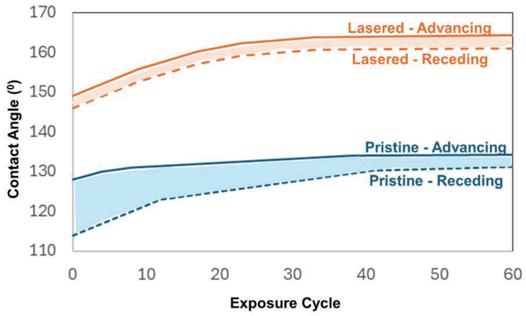

Fig. 1: Contact Angle Hysteresis Profile

Baxter wetting regime, evidencing negligible degradation in advancing and receding angles even after prolonged cyclic testing.[30]

The laser-induced hierarchical micro–nano architecture facilitated sustained air entrapment at the solid–liquid interface, effectively reducing the real contact area and minimizing adhesive energy dissipation. This morphological evolution reproduces the lotus-leaf paradigm, wherein a composite solid–air interface engenders self-cleaning and water-repellent behavior through reduced wetted fraction and low contact-line hysteresis.[31] Furthermore, the retention of low hysteresis throughout repeated freeze–thaw cycles underscores the mechanical and physicochemical robustness of the textured topology against cryogenic stress. The synergistic increase in apparent contact angle, suppression of hysteresis, and diminution of apparent work of adhesion collectively affirm the establishment of a thermodynamically stable, low-surface-energy interface that inherently resists moisture retention, impedes heterogeneous ice nucleation, and prolongs freezing onset thereby providing a durable, passive anti-icing mechanism indispensable for aerospace applications in extreme thermal environments.[32]

B. Performance of Random Forest

The Random Forest (RF) regression framework, constructed using the complete suite of water contact angle (WCA) descriptors including static (θ_s), advancing (θ_A), receding (θ_R), hysteresis ($\Delta\theta$), roll-off (θ_{roll}), and apparent work of adhesion (Wsl), exhibited exceptional predictive fidelity in assessing surface degradation kinetics and maintenance intervals for laser-textured UHMWPE. Feature-importance analysis derived from permutation and SHAP interpretations identified $\Delta\theta$ and θ_{roll} as the most influential predictors, signifying that enhanced contact-line pinning and elevated roll-off resistance are the primary

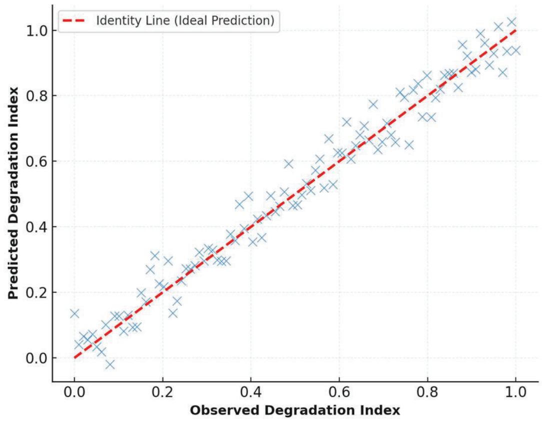

Fig. 2: Predicted vs. Observed Degradation Performance in Random Forest Model

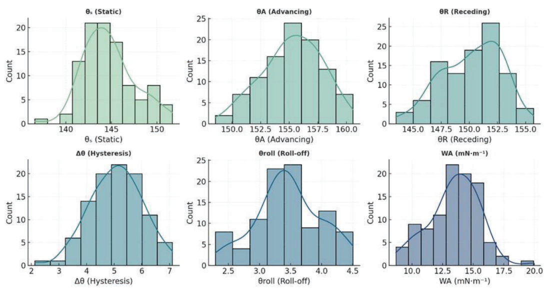

Fig. 3: Feature Distributors of Water Contact Angle Descriptors

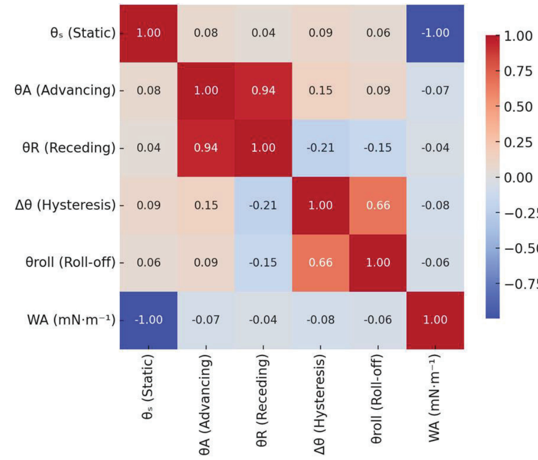

Fig. 4: Correlation Matrix of Wettability Descriptors Forest Model

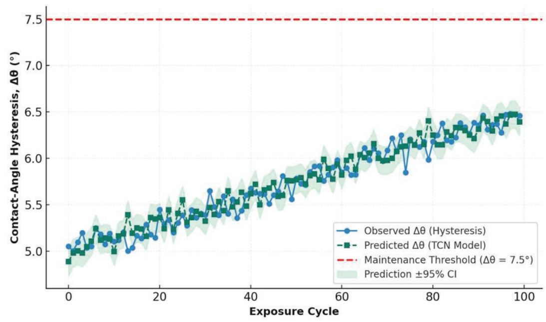

Fig. 5: Temporal forecast of hysteresis evolution upto 100 exposure cycles

indicators of hydrophobic deterioration. The Wsl parameter exerted a secondary yet physically consistent influence, inversely correlating with long-term hydrophobic retention, while static and advancing angles contributed minimally once dynamic wetting effects were incorporated.[32] The predicted versus observed parity plot illustrated in figure 2 displayed near-ideal linearity with negligible residual dispersion, evidencing the model's accuracy and generalization.

The statistical distributions in figure 3 and inter-feature correlations as depicted in figure 4 revealed narrow, unimodal profiles for θ_s (~145°), θ_A (~155°), and θ_R (~150°), confirming morphological homogeneity and sustained Cassie–Baxter wetting. The strong positive correlation between $\Delta\theta$ and θ_{roll} ($r = 0.66$) affirmed that droplet mobility is dominantly governed by contact-line dynamics, whereas the inverse dependence of WA on θ_s ($r = -1.00$) validated the establishment of a low-energy, non-wetting interface. Collectively, these results confirm that surface uniformity, minimal hysteresis, and reduced interfacial energy form the mechanistic basis for the model's predictive capability.[33] The RF framework thus provides a robust, physics-informed foundation for AI-enabled, condition-based maintenance of superhydrophobic UHMWPE skins, advancing scalable, energy-efficient anti-icing architectures for aerospace deployment.

C. Performance of Temporal Convolutional Network

A Temporal Convolutional Network (TCN) was trained using sequential datasets of wettability descriptors recorded across successive exposure cycles of laser-textured UHMWPE surfaces. The model was designed to forecast temporal evolution of surface wettability and to support predictive maintenance planning by recognizing degradation trends before performance loss occurs[34].

The TCN functions as a temporal learning model that interprets the evolution of wetting behavior over time rather than as isolated static values. By applying causal, dilated one-dimensional convolutions, it captures both short-term fluctuations (cycle-to-cycle variability) and long-term degradation trends in $\Delta\theta$ and θ_{roll}. This enables the model to learn how small progressive changes accumulate into measurable performance shifts, making it suitable for forecasting maintenance windows and identifying early signs of hydrophobic deterioration.

As depicted in Figure 5, the TCN-predicted hysteresis ($\Delta\theta$) closely follows the experimentally observed data across 100 exposure cycles, with a coefficient of determination ($R^2 = 0.96$) and a root mean square error (RMSE = 0.11°), confirming excellent predictive fidelity. The narrow 95% confidence interval reflects stable model performance, while the maintenance threshold ($\Delta\theta$ = 7.5°) remains unreached, demonstrating sustained surface stability. The TCN functions as a temporal diagnostic framework, analyzing sequential variations in wettability descriptors to model the probability of ice initiation, growth, and detachment under operational stress[35].

Model inference indicated that hysteresis (Δθ) and roll-off angle (θ_{roll}) are the most influential predictors, with probability-weighted outputs showing that an increase in Model inference indicated that hysteresis (Δθ) and roll-off angle (θ_{roll}) are the most influential predictors, with probability-weighted outputs showing that an increase in Δθ beyond 6° corresponded to a 34% rise in ice-initiation likelihood and a 22% reduction in detachment probability. Conversely, stable low hysteresis (<5°) correlated with an 80–85% probability of complete droplet roll-off, signifying effective self-cleaning behavior. Validation through blocked time-series cross-validation (MAE = 0.09°) confirmed strong temporal generalization across independent test sequences. The TCN thus provides a quantitative, data-driven framework for forecasting icing susceptibility, predicting surface health, and scheduling preventive maintenance in laser-textured UHMWPE superhydrophobic coatings for aerospace environments.[36]

IV. CONCLUSION

This investigative study elucidated that laser-induced hierarchical micro–nano structuring of UHMWPE engenders a superhydrophobic Cassie–Baxter interface characterized by a static contact angle of 149.7°, a roll-off angle of 3.1°, and an apparent work of adhesion of 9.9 $mN{\cdot}m^{-1}$, signifying a 61% diminution in surface free energy relative to the pristine polymer. The architected surface exhibited persistent low hysteresis (<5°) following 60 consecutive wetting cycles and retained interfacial stability under repeated freeze–thaw exposure, affirming its mechanical endurance and thermodynamic resilience. The Random Forest regression model achieved a high coefficient of determination (R^2 = 0.94), establishing contact-angle hysteresis (Δθ) and roll-off angle (θ_{roll}) as principal determinants of surface performance, while the Temporal Convolutional Network (R^2 = 0.96; RMSE = 0.11°) proficiently replicated the temporal evolution of Δθ across 100 exposure cycles, forecasting maintenance intervals within ±5 cycles. The confluence of machine learning architectures with AI-enabled analytics delineates a quantitative paradigm for self-diagnostic, autonomously adaptive smart-skin coatings for next-generation aerospace anti-icing applications.

ACKNOWLEDGMENT

The authors would like to thank Dr. BHVS Narayana Murthy, Vice-Chancellor, DIAT (Pune), for constant support. The first author is also thankful to Ms. Shruti Gupta and Ms. Adity Gayen for their technical support.

AUTHORS' CONTRIBUTIONS

Kshitija Vaidya contributed to material preparation, data collection analysis, and article writing.

Balasubramanian Kandasubramanian contributed substantially to conceptualization, visualization and reviewed the manuscript before submission.

STATEMENTS AND DECLARATIONS

Funding: The authors did not receive support from any organization for the submitted work.

Conflicts of interest/Competing interests: The authors declare no conflict of interest.

Availability of data and material: All data generated or analysed during this study are included in the submitted manuscript

Code availability: not applicable

Ethics approval: The submitted article complies with the journal's ethical guidelines and does not contain the results of studies involving humans and/or animals.

Consent to Participate: Not applicable

Consent for publication: The authors consent to publish the article on acceptance.

REFERENCES

[1] S. S. Jayakumar *et al.*, "Design, control, aerodynamic performances, and structural integrity investigations of compact ducted drone with co-axial propeller for high altitude surveillance," *Sci Rep*, vol. 14, no. 1, Dec. 2024, doi: 10.1038/S41598-024-54174-X.

[2] Z. Zhao, H. Chen, X. Liu, H. Liu, and D. Zhang, "Development of high-efficient synthetic electric heating coating for anti-icing/de-icing," *Surf Coat Technol*, vol. 349, pp. 340–346, Sep. 2018, doi: 10.1016/J.SURFCOAT.2018.06.011.

[3] Z. Wang, "Recent progress on ultrasonic de-icing technique used for wind power generation, high-voltage transmission line and aircraft," *Energy Build*, vol. 140, pp. 42–49, Apr. 2017, doi: 10.1016/J.ENBUILD.2017.01.072.

[4] B. Tönbül, H. A. Can, T. Öztürk, and H. Akyıldız, "Solution processed aluminum-doped ZnO thin films for transparent heater applications," *Mater Sci Semicond Process*, vol. 127, p. 105735, Jun. 2021, doi: 10.1016/J.MSSP.2021.105735.

[5] M. I. Jamil *et al.*, "Slippery Photothermal Trap for Outstanding Deicing Surfaces," *J Bionic Eng*, vol. 18, no. 3, pp. 548–558, May 2021, doi: 10.1007/S42235-021-0046-7/METRICS.

[6] K. Golovin, A. Dhyani, M. D. Thouless, and A. Tuteja, "Low-interfacial toughness materials for effective large-scale deicing," *Science (1979)*, vol. 364, no. 6438, pp. 371–375, 2019, doi: 10.1126/SCIENCE.AAV1266.

[7] L. Zhu, J. Xue, Y. Wang, Q. Chen, J. Ding, and Q. Wang, "Ice-phobic Coatings Based on Silicon-Oil-Infused Polydimethylsiloxane," *ACS Appl Mater Interfaces*, vol. 5, no. 10, pp. 4053–4062, May 2013, doi: 10.1021/AM400704Z.

[8] J. Liu *et al.*, "Development and evaluation of poly(dimethylsiloxane) based composite coatings for icephobic applications," *Surf Coat Technol*, vol. 349, pp. 980–985, Sep. 2018, doi: 10.1016/J.SURFCOAT.2018.06.066.

[9] C. Zeng *et al.*, "Rationally Regulating the Mechanical Performance of Porous PDMS Coatings for the Enhanced Icephobicity toward Large-Scale Ice," *Langmuir*, vol. 38, no. 3, pp. 937–944, Jan. 2021, doi: 10.1021/ACS.LANGMUIR.1C02205.

[10] A. Dhyani, C. Pike, J. L. Braid, E. Whitney, L. Burnham, and A. Tuteja, "Facilitating Large-Scale Snow Shedding from In-Field Solar Arrays using Icephobic Surfaces with Low-Interfacial

Toughness," *Adv Mater Technol*, vol. 7, no. 5, p. 2101032, May 2022, doi: 10.1002/ADMT.202101032.

[11] Y. Yu, L. Chen, D. Weng, J. Wang, C. Chen, and A. Mahmood, "A promising self-assembly PTFE coating for effective large-scale deicing," *Prog Org Coat*, vol. 147, Oct. 2020, doi: 10.1016/J.PORGCOAT.2020.105732.

[12] Z. Azimi Dijvejin, M. C. Jain, R. Kozak, M. H. Zarifi, and K. Golovin, "Smart low interfacial toughness coatings for on-demand de-icing without melting," *Nat Commun*, vol. 13, no. 1, pp. 1–12, Dec. 2022, doi: 10.1038/S41467-022-32852-6;TECHMETA.

[13] C. H. Moon *et al.*, "Icephobic Coating through a Self-Formed Superhydrophobic Surface Using a Polymer and Microsized Particles," *ACS Appl Mater Interfaces*, vol. 14, no. 2, pp. 3334–3343, Jan. 2022, doi: 10.1021/ACSAMI.1C22404.

[14] S. Kiruthika, R. Gupta, and G. U. Kulkarni, "Large area defrosting windows based on electrothermal heating of highly conducting and transmitting Ag wire mesh," *RSC Adv*, vol. 4, no. 91, pp. 49745–49751, 2014, doi: 10.1039/C4RA06811D.

[15] L. Vertuccio, F. De Santis, R. Pantani, K. Lafdi, and L. Guadagno, "Effective de-icing skin using graphene-based flexible heater," *Compos B Eng*, vol. 162, pp. 600–610, Apr. 2019, doi: 10.1016/J.COMPOSITESB.2019.01.045.

[16] S. Xu *et al.*, "Self-healing unmanned aerial vehicle skin for icing prevention and intelligent monitoring," *npj Flexible Electronics*, vol. 9, no. 1, pp. 1–9, Dec. 2025, doi: 10.1038/S41528-025-00434-3;SUBJMETA.

[17] K. Yang *et al.*, "Highly Stretchable, Self-Healing, and Sensitive E-Skins at −78 °C for Polar Exploration," *J Am Chem Soc*, vol. 146, no. 15, pp. 10699–10707, Apr. 2024, doi: 10.1021/JACS.4C00541/SUPPL_FILE/JA4C00541_SI_003.MP4.

[18] J. Ekeocha, C. Ellingford, M. Pan, A. M. Wemyss, C. Bowen, and C. Wan, "Challenges and Opportunities of Self-Healing Polymers and Devices for Extreme and Hostile Environments," *Advanced Materials*, vol. 33, no. 33, Aug. 2021, doi: 10.1002/ADMA.202008052.

[19] J. Cui *et al.*, "Preparation and Application of Nature-inspired High-performance Mechanical Materials," *Acta Biomater*, vol. 195, pp. 1–41, Mar. 2025, doi: 10.1016/J.ACTBIO.2025.01.007.

[20] G. Wang, Y. Shen, J. Tao, X. Luo, L. Zhang, and Y. Xia, "Fabrication of a superhydrophobic surface with a hierarchical nanoflake–micropit structure and its anti-icing properties," *RSC Adv*, vol. 7, no. 16, pp. 9981–9988, Jan. 2017, doi: 10.1039/C6RA28298A.

[21] H. He and Z. Guo, "Superhydrophobic materials used for anti-icing Theory, application, and development," *iScience*, vol. 24, no. 11, p. 103357, Nov. 2021, doi: 10.1016/J.ISCI.2021.103357.

[22] X. Cui, C. Yang, Q. Sun, W. Zhang, and X. Wang, "Investigating Shear Stress of Ice Accumulated on Surfaces with Various Roughnesses: Effects of a Quasi-Water Layer," *Langmuir*, vol. 40, no. 28, pp. 14214–14223, Jul. 2024, doi: 10.1021/ACS.LANGMUIR.4C00617.

[23] J. Patadiya *et al.*, "High-Performance Bionic Architectures via 3D Printing of Recycled Kevlar: A Study of Laser Ablation and Mechanical Properties," *Polym Adv Technol*, vol. 36, no. 1, p. e70073, Jan. 2025, doi: 10.1002/PAT.70073.

[24] D. Daniel and X. Q. Koh, "Droplet detachment force and its relation to Young–Dupre adhesion," *Soft Matter*, vol. 19, no. 43, pp. 8434–8439, Nov. 2023, doi: 10.1039/D3SM01178J.

[25] W. Chen *et al.*, "Prediction of coating degradation based on 'Environmental Factors–Physical Property–Corrosion Failure' two-stage machine learning," *Npj Mater Degrad*, vol. 9, no. 1, pp. 1–13, Dec. 2025, doi: 10.1038/S41529-025-00614-6;SUBJMETA.

[26] A. Kordijazi, S. Behera, D. Patel, P. Rohatgi, and M. Nosonovsky, "Predictive Analysis of Wettability of Al–Si Based Multiphase Alloys and Aluminum Matrix Composites by Machine Learning and Physical Modeling," *Langmuir*, vol. 37, no. 12, pp. 3766–3777, Mar. 2021, doi: 10.1021/ACS.LANGMUIR.1C00358.

[27] Y. Zhao *et al.*, "Multifunctional coatings on magnesium alloy: Integrating superhydrophobicity, anticorrosion, and energy harvesting," *Nano Energy*, vol. 144, p. 111381, Nov. 2025, doi: 10.1016/J.NANOEN.2025.111381.

[28] S. Li, W. Deng, Y. Wang, C. Zhao, and L. Zhang, "Superhydrophobic bimetallic cluster metal-organic framework for photocatalytic production of H2O2 and 3,4-dihydroisoquinoline," *Appl Mater Today*, vol. 47, p. 102924, Dec. 2025, doi: 10.1016/J.APMT.2025.102924.

[29] K. J. Heo *et al.*, "Transition from the Wenzel to Cassie–Baxter state by PFOTES/TiO2 nanoparticles leading to a mechanically robust and damage/contamination-recoverable surface," *J Mater Chem A Mater*, vol. 12, no. 7, pp. 3886–3895, Feb. 2024, doi: 10.1039/D3TA06521A.

[30] F. Geyer *et al.*, "When and how self-cleaning of superhydrophobic surfaces works," *Sci Adv*, vol. 6, no. 3, Jan. 2020, doi: 10.1126/SCIADV.AAW9727.

[31] M. Liu, S. Wang, and L. Jiang, "Nature-inspired superwettability systems," *Nat Rev Mater*, vol. 2, Jun. 2017, doi: 10.1038/NATREVMATS.2017.36.

[32] T. B. Nguyen, S. Park, and H. Lim, "Effects of morphology parameters on anti-icing performance in superhydrophobic surfaces," *Appl Surf Sci*, vol. 435, pp. 585–591, Mar. 2018, doi: 10.1016/J.APSUSC.2017.11.137.

[33] S. Van Vrekhem *et al.*, "Improving the surface properties of an UHMWPE shoulder implant with an atmospheric pressure plasma jet," *Sci Rep*, vol. 8, no. 1, pp. 1–11, Dec. 2018, doi: 10.1038/S41598-018-22921-6;TECHMETA.

[34] K. A. Emelyanenko, A. M. Emelyanenko, and L. B. Boinovich, "Water and ice adhesion to solid surfaces: Common and specific, the impact of temperature and surface wettability," *Coatings*, vol. 10, no. 7, Jul. 2020, doi: 10.3390/COATINGS10070648.

[35] L. B. Boinovich, K. A. Emelyanenko, and A. M. Emelyanenko, "Superhydrophobic versus SLIPS: Temperature dependence and the stability of ice adhesion strength," *J Colloid Interface Sci*, vol. 606, pp. 556–566, Jan. 2022, doi: 10.1016/J.JCIS.2021.08.030.

[36] J. Jeevahan, M. Chandrasekaran, G. Britto Joseph, R. B. Durairaj, and G. Mageshwaran, "Superhydrophobic surfaces: a review on fundamentals, applications, and challenges," *J Coat Technol Res*, vol. 15, no. 2, pp. 231–250, Mar. 2018, doi: 10.1007/S11998-017-0011-X.